Journal Pre-proof

Elucidating elusive quaternary selenide $EuCeCuSe_3$: Synthesis, crystal structure, properties and theoretical studies

Maxim V. Grigoriev, Anna V. Ruseikina, Maxim S. Molokeev, Vladimir A. Chernyshev, Aleksandr S. Aleksandrovsky, Alexander S. Krylov, Svetlana N. Krylova, Nikolai P. Shestakov, Dmitriy A. Velikanov, Alexander A. Garmonov, Alexey V. Matigorov, Evgeny A. Ostapchuk, Thomas Schleid, Damir A. Safin

PII: S1002-0721(22)00320-9

DOI: https://doi.org/10.1016/j.jre.2022.11.004

Reference: JRE 1349

To appear in: *Journal of Rare Earths*

Received Date: 13 August 2022

Revised Date: 24 October 2022

Accepted Date: 7 November 2022

Please cite this article as: Grigoriev MV, Ruseikina AV, Molokeev MS, Chernyshev Vladimir.A., Aleksandrovsky AS, Krylov AS, Krylova SN, Shestakov NP, Velikanov Dmitriy.A., Garmonov AA, Matigorov AV, Ostapchuk EA, Schleid T, Safin DA, Elucidating elusive quaternary selenide $EuCeCuSe_3$: Synthesis, crystal structure, properties and theoretical studies, *Journal of Rare Earths* (2022), doi: https://doi.org/10.1016/j.jre.2022.11.004.

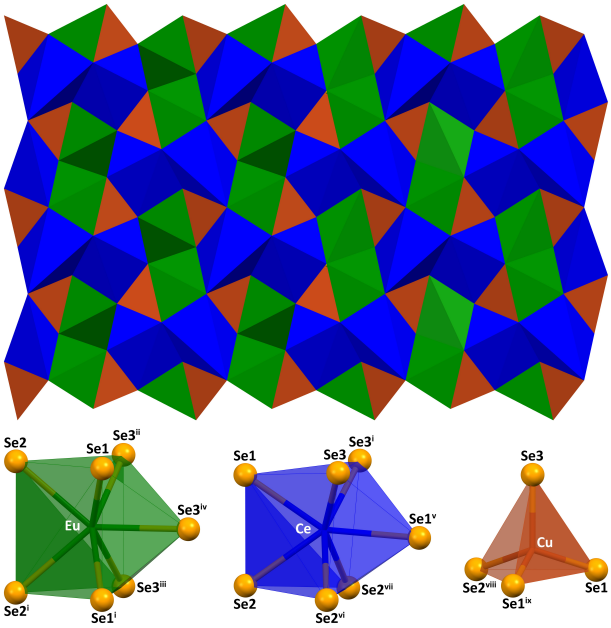

Elucidating elusive quaternary selenide $EuCeCuSe_3$: Synthesis, crystal structure, properties and theoretical studies

Maxim V. Grigoriev[a], Anna V. Ruseikina[a,*], Maxim S. Molokeev[b,c,d], Vladimir A. Chernyshev[e], Aleksandr S. Aleksandrovsky[c,f], Alexander S. Krylov[c], Svetlana N. Krylova[c], Nikolai P. Shestakov[c], Dmitriy A. Velikanov[c], Alexander A. Garmonov[g], Alexey V. Matigorov[a], Evgeny A. Ostapchuk[a], Thomas Schleid[h], Damir A. Safin[i,j,k,*]

[a] *Laboratory of Theory and Optimization of Chemical and Technological Processes, University of Tyumen, Volodarskogo Str. 6, 625003 Tyumen, Russian Federation*

[b] *Research and Development Department, Kemerovo State University, Krasnaya Str. 6, 650000 Kemerovo, Russian Federation*

[c] *Kirensky Institute of Physics, Federal Research Center KSC SB RAS, Akademgorodok 50 bld. 38, 660036 Krasnoyarsk, Russian Federation*

[d] *Department of Physics, Far Eastern State Transport University, Serysheva str. 47, 680021 Khabarovsk, Russian Federation*

[e] *Institute of Natural Sciences and Mathematics, Ural Federal University named after the First President of Russia B.N. Yeltsin, Mira Str. 19, 620002 Ekaterinburg, Russian Federation*

[f] *Department of Photonics and Laser Technology, Siberian Federal University, Svobodnii ave. 79, 660079 Krasnoyarsk, Russian Federation*

[g] *Institute of Physics and Technology, University of Tyumen, Volodarskogo Str. 6, 625003 Tyumen, Russian Federation*

[h] *Institute for Inorganic Chemistry, University of Stuttgart, Pfaffenwaldring 55, D-70569 Stuttgart, Germany*

[i] *Advanced Materials for Industry and Biomedicine Laboratory, Kurgan State University, Sovetskaya Str. 63/4, 640020 Kurgan, Russian Federation*

[j] *Innovation Center for Chemical and Pharmaceutical Technologies, Ural Federal University named after the First President of Russia B.N. Yeltsin, Mira Str. 19, 620002 Ekaterinburg, Russian Federation*

[k] *University of Tyumen, Volodarskogo Str. 6, 625003 Tyumen, Russian Federation*

☆ **Foundation item:** Project supported by the Tyumen Oblast Government, as part of the West-Siberian Interregional Science and Education Center's (89-DON (3)) and state assignment of the Ministry of Science and Higher Education of the Russian Federation (720000Ф.99.1.Б385АА13000).

* Corresponding author. Telephone number: +7 3452 597 467

E-mail addresses: a.v.rusejkina@utmn.ru (A.V. Ruseikina), damir.a.safin@gmail.com (D.A. Safin)

Abstract We report on the novel heterometallic quaternary selenide $EuCeCuSe_3$, the fabrication of which has been a challenge until this work. The structure of the reported selenide was elucidated from the powder X-ray diffraction data, which revealed the formation of $EuCeCuSe_3$ with excellent yield (96.7%) accompanied with a minor fraction of $CeSe_2$ (3.3%), and was best solved in orthorhombic space group *Pnma* with the $BaLaCuS_3$ structural type. Thus, the crystal structure of the title compound completes the row of the heterometallic quaternary selenides $EuRECuSe_3$ (RE = La, Pr, Nd, Sm, Eu, Gd, Tb, Dy, Ho, Er, Tm, Yb, Lu, Y), of which the cerium-based derivative exclusively belongs to the $BaLaCuS_3$ structural type. The distortion of the $CuSe_4$ polyhedron was compared for the whole series of $EuRECuSe_3$ compounds using the τ_4-descriptor for four coordinated ions, which revealed the highest degree of distortion for the Ce^{3+}-containing selenide, followed by the La^{3+}-based derivative. Furthermore, the crystallographic and geometrical parameters of the reported selenide were discussed in comparison to the Ce^{3+}-based sulfides $SrCeCuS_3$ and $EuCeCuS_3$. *Ab initio* calculations of the crystal structure, a phonon spectrum and elastic constants for the crystal of $EuCeCuSe_3$ were also performed. The types and wavenumbers of fundamental modes were determined and the involvement of ions participating in the phonon modes was assessed. The experimental IR spectrum of the reported selenide was interpreted and found to be in agreement with the calculated spectrum. The experimental direct band gap of $EuCeCuSe_3$ was measured to be 1.36 eV that is consistent with the concept of its origin due to interband transitions between orbitals emerging mainly from 4f (valence band) and 5d (conduction band) levels of the Eu^{2+} cation. The dependence of the Young's modulus on the direction demonstrates the anisotropy of the elastic properties, while the Vickers hardness for $EuCeCuSe_3$ was calculated to be 5.2 GPa. Finally, the title compound is paramagnetic above 4 K.

Keywords: Quaternary selenide; Synthesis; Crystal structure; *Ab initio* calculations; Magnetic measurements; Spectroscopy.

1. Introduction

Materials based on cerium chalcogenides are wide-gap semiconductors with a broad transparency range and a high refractive index[1–3]. They possess excellent photo- and electrocatalytic activities[4,5] and exhibit strong blue radiation, which is of potential use in the production of light emitting diodes (LEDs)[5]. Furthermore, they are used in the production of refractory materials and ceramic powders, radioceramics, phosphors, solid electrolytes, modifiers, carriers and catalysts[6–8]. Cerium sesquiselenide exhibits the highest value of the Faraday rotation in comparison to the selenides of the other rare earth element sesquiselenides, approaching the record value for paramagnets[3,9]. Cerium sulfides and selenides have an anomalously low band gap within the chalcogenides of other lanthanides, since the absorption edge is determined by transitions from the 4f band to the conduction band (5d(Ln)), which in cerium chalcogenides is located above the valence band (3p(S) or 4p(Se))[3,10].

Comprehensive studies of the quaternary cerium chalcogenides suggest that phase stabilization is more favourable, when copper is used as the transition metal, which is explained by the mobile nature of the Cu^+ cations even at low temperatures. This promotes ion diffusion over long distances and facilitates its rapid achievement of thermodynamic phase minima[11]. Using copper in the synthetic chemistry of cerium chalcogenides has already allowed to produce a series of quaternary compounds[11–24]. Notably, the Cu^+ cations determine the semiconductor properties of complex chalcogenides, while metallic conductivity is expected in chalcogenides containing both the Cu^+ and Cu^{2+} cations[14]. However, the latter ion is unstable in the presence of the S^{2-} and Se^{2-} anions[12,25]. Interesting structural and physical properties of quaternary cerium chalcogenides arise due to the combination of the covalent nature of transition metal-chalcogen bonds with the more ionic nature of lanthanide-chalcogen bonds[23]. These compounds have channel-like or layered structures[26] as well as exhibit a variety of properties such as *p*-type semiconductors[11,12,14,27], ferromagnetics[24], antiferromagnetics [12,14] and paramagnetics[12,13,28]. They exhibit metallic[11] or metalloid[14] character and melt incongruently at 1468–1524 K[21,24].

Cerium-based quaternary selenides $ACeCuSe_3$ (A = Sr[16,17], Ba[13]) and quaternary sulfides $ACeCuS_3$ (A = Eu[20,22,24], Sr[19,21], Ba[13]) crystallize in three orthorhombic structural types, namely Ba_2MnS_3[16,19,24], $BaLaCuS_3$[19,24] and Eu_2CuS_3[13] with space group *Pnma*. For the sulfides $ACeCuS_3$ (A = Sr, Eu), a change of the structural type from $BaLaCuS_3$ to Ba_2MnS_3 was revealed in the temperature range 970–1170 K[19,24]. In the resulting structures, the A^{2+} and Ce^{3+} cations can occupy either the same[16,19,20] or different crystallographic positions[13]. The calculated band gap of $ACeCuCh_3$ (A = Eu, Sr, Ba, Ch = S, Se) is lower for selenides (0.446–1.161 eV) than for the corresponding sulfides (1.060–1.312 eV)[29].

The presence of Eu^{2+} cations in the quaternary compounds allows to vary the values of the band gap[30]. Polycrystals of orthorhombic selenides $EuRECuSe_3$ (RE = La, Sm–Lu) were obtained recently and their optical and magnetic properties were characterized in detail[31]. These compounds are ferro- and ferrimagnets with transition temperatures of 4.7–6.3 K and with direct optical band gaps of 1.07–2.09 eV[31]. However, the cerium-based heterometallic quaternary selenide $EuCeCuSe_3$ has been elusive so far. The synthetic pathway toward $EuRECuSe_3$ is based on dissolving the rare earth element oxides in nitric acid[31]. However, CeO_2 is poorly soluble in nitric acid and requires reducing agents to improve its solubility[32].

With all this in mind, in this work we have focused on the synthesis of $EuCeCuSe_3$ as well as on studies of its crystal structure, magnetic and optical properties. The obtained results were verified with *ab initio* calculations. Fabrication of the title selenide allowed to complete the row of the heterometallic quartenary selenides $EuRECuSe_3$ (RE = La, Pr, Nd, Sm, Eu, Gd, Tb, Dy, Ho, Er, Tm, Yb, Lu, Y). It should be noted that these quaternary selenides, comprising copper and rare earth elements, are of particular interest nowadays due to a variety of different combinations of cations that enable the design of structural type and band gap, as well as electrical and optical characteristics, thus attracting an ever increasing attention for practical application.

2. Experimental

2.1. Materials

Eu_2O_3 (99.9%) and CeO_2 (99.95%) were purchased from the Uralredmet manufacture (Verkhnyaya Pyshma, Russian Federation). Selenium (extra-pure grade, 17-4) and $CuSO_4 \cdot 5H_2O$ (pure for analysis) were purchased from Lenreactiv, CJSC (Saint Petersburg, Russian Federation). H_2O_2 (37%, extra-pure grade, 8-4 specifications 2611-003-25665344-2008) was purchased from EKOS-1, JSC (Moscow, Russian Federation), and copper (99.9%) was obtained from SZB Tsvetmet, OJSC (Saint Petersburg, Russian Federation). Concentrated nitric acid (extra-pure grade, 18-4 all-Union State Standard 11125-84) was purchased from Chemreaktivsnab, CJSC (Ufa, Russian Federation). Activated charcoal was obtained from Tyumenskie Ssistemy Vodoochistki, Ltd. (Tyumen, Russian Federation).

2.2. Physical measurements

The powder X-ray diffraction data (Fig. 1) were collected at room temperature with a ДРОН 7 (Burevestnik, Saint Petersburg, Russia) powder diffractometer (Cu-Kα radiation, graphite monochromator). The step size of 2θ was 0.02°, and the counting time 10 s per step. Analysis of systematic extinctions revealed that $EuCeCuSe_3$ crystallized in orthorhombic space group *Pnma*. Almost all peaks were indexed in an orthorhombic cell with parameters close to those of $BaLaCuS_3$[13,33]. Thus, the latter sulfide was used as an initial structural model for the Rietveld refinement, which was performed using TOPAS 4.2[34]. The Ba, La and S atoms in the structural model were replaced with Eu, Ce and Se, respectively. The final refinement was stable with low *R*-factors: R_{wp} = 5.78%, R_p = 4.54%, χ^2 = 1.39, R_B = 1.78%. The refinement of the powder pattern (Fig. 1) allowed to reveal a minor second phase of $CeSe_2$ (3.3%). The crystal structure was visualized with the program package Diamond 3[35]. CCDC 2189101 contains supplementary crystallographic data. These data can be obtained free of charge via https://www.ccdc.cam.ac.uk/structures or from the Cambridge Crystallographic Data Centre, 12 Union Road, Cambridge CB2 1EZ, UK (fax: (+44)-1223-336-033 or e-mail: deposit@ccdc.cam.ac.uk).

Fig. 1. Observed (black) and calculated (red) X-ray powder diffraction patterns for $EuCeCuSe_3$ and their difference (grey) after crystal structure refinement.

Scanning electron microscopy (SEM) was performed on a JEOLJSM-6510 LV microscope (JEOL Ltd., Tokyo, Japan) equipped with an energy dispersive spectrometer. Fourier-transform infrared (FTIR) absorption spectra in the range of 60–675 cm^{-1} were recorded on a VERTEX 80v FT-IR spectrometer (Bruker OJSC, Germany). The attenuated total reflectance infrared (ATR-IR) absorption spectra in the range of 400–4000 cm^{-1} were recorded on a Cary 630 FTIR spectrometer (Agilent Technologies Inc., Santa Clara, CA, USA) equipped with an ATR attachment and a DTGS detector. Diffuse reflectance spectra were recorded on a UV-2600 spectrophotometer (Shimadzu OJSC, Tokyo, Japan) equipped with an ISR-2600Plus attachment with the photomultiplier PMT of the R-928 type and InGaAs detectors. $BaSO_4$ (99.8%) was used as a standard. Gaseous hydrogen was obtained on a SPEKTR 16 4D hydrogen generator (Spektr Ltd., Petrozavodsk, Russian Federation). The temperature in the electric heating furnaces used for synthesis was controlled using a Termodat-16K6 (InSAT Ltd., Moscow, Russian Federation) temperature controller with a chromel-alumel thermocouple. The low-temperature (4.2–65 K) magnetic susceptibilities of $EuCeCuSe_3$ (0.040 g) were studied on a SQUID magnetometer (Kirensky Institute of Physics, Krasnoyarsk, Russian Federation)[36,37] in a 796 A/m magnetic field. The measurements of low-temperature magnetization were performed in the zero-field cooled (ZFC) and nonzero-field cooled (FC) modes. The room-temperature magnetic properties were studied on a vibrating sample magnetometer with a Puzey electromagnet[38]. The magnetic field was varied in the range from –1.2 to 1.2 mA/m. The magnetometer signal from the container and the lid were measured separately and then subtracted from the total signal. A powdered sample of $EuCeCuSe_3$ (0.0699 g) was tightly packed into the polyvinylchloride container of 4.2 mm in diameter and 5.6 mm height with the lid.

2.3. DFT calculations

The density functional theory (DFT) calculations were carried out using the PBE0 and B3LYP hybrid functionals, which consider both local and nonlocal Hartree-Fock exchanges. The calculations were performed using the CRYSTAL17 program designed to simulate periodic structures[39]. For Eu^{3+}, the ECP53MWB quasirelativistic pseudopotential was used with the attached valence basis set ECP53MWB[40]. For Ce^{3+}, the ECP*n*MWB quasirelativistic pseudopotential was used with the attached valence basis set ECP*n*MWB-I (*n* = 48 and is a number of core electrons)[40]. Thus, the inner shells of each rare earth metal cation, including 4f, were replaced by a pseudopotential. To describe the outer shells $5s^25p^6$, involved in chemical bonding, valence basis sets were used. Such an approach makes it possible to reconstitute successfully both the lattice structure and the dynamics in compounds that have a lanthanide cation sublattice[24]. For copper and selenium, we used full-electron basis sets, known in the CRYSTAL program site as Cu_86-4111(41D)G_doll_2000 and Se_976-311d51G_towler_1995, respectively[39]. Gaussian primitives with orbital-exponent values less than 0.1 were removed from basis sets since these calculations are periodic. The exponent in the outer p-orbital of the selenium basis set was set to 0.1742. The accuracy of calculation of the self-consistent field and the two-electron integrals was set at 10^{-9} and 10^{-8} a.u., respectively. Integration over the Brillouin zone was carried out according to the Monkhorst-Pack scheme with a grid of *k*-points equal to 8 × 8 × 8.

The sequence of the DFT calculations was as follows: the crystal structure was first optimized followed by the calculation of the phonon spectrum at the Γ point or the elastic constants.

2.4. Synthesis

A powder sample of $EuCeCuSe_3$ was prepared by reductive selenidation of the oxide mixtures in a flow of H_2 and H_2Se at 970–1020 K for 8 h according to a slightly modified synthetic procedure reported recently[31]. Particularly, the preparation of the samples of Eu_2O_3 and metallic copper as well as their dissolving in nitric acid were achieved according to the reported procedure[31], while CeO_2 was preliminarily annealed in silica glass in a muffle furnace at 770 K to remove sorption water, hydroxides and carbonates[41,42], followed by dissolving in the same acid by a dropwise addition of H_2O_2 until CeO_2 was completely dissolved. Thus, interaction of the parent reagents proceeded according to the following reaction (Eq. (1)):

$$Eu_2O_3 + 2CeO_2 + 2Cu + H_2O_2 + 20HNO_3 \rightarrow 2Eu(NO_3)_3 + 2Ce(NO_3)_3 + 2Cu(NO_3)_2 + 11H_2O + O_2 + 4NO_2 \quad (1)$$

The resulting product $EuCeCuSe_3$ was examined by SEM-EDX and the obtained data were in good agreement with the powder X-ray diffraction data and are collected in Table 1.

Table 1. The calculated and found elemental analysis data for $EuCeCuSe_3$ obtained using SEM-EDX.

Compound (in mass fraction)	Calculated (%)				Found (%)			
	Eu	Ce	Cu	Se	Eu	Ce	Cu	Se
$EuCeCuSe_3$	25.65	23.65	10.72	39.98	24.89	24.39	10.39	40.33
96.7% $EuCeCuSe_3$ + 3.3% $CeSe_2$	25.21	24.04	10.54	40.20				

3. Results and discussion

3.1. Synthesis of $EuCeCuSe_3$

The heterometallic quaternary selenide $EuCeCuSe_3$ was obtained according to the recently reported synthetic procedure applied for other derivatives of the $EuRECuSe_3$ series (RE = La, Sm, Eu, Gd, Tb, Dy, Ho, Er, Tm, Yb, Lu, Y)[31]. Eu_2O_3 and CeO_2 were preliminary annealed at 1070 and 770 K, respectively, to remove sorption water, hydroxides and carbonates[41,42], while copper fragments were mechanically cleaned, treated with alcohol and dried at room temperature. Then the co-crystallized nitrates of Eu^{3+}, Ce^{3+} and Cu^{2+} were produced by dissolving the educts in concentrated nitric acid and hydrogen peroxide upon heating. The final

residue was subjected to thermolysis, and its completeness was monitored by IR spectroscopy and the distribution spectra of elements, plotted using an energy dispersive analysis system. According to a X-ray phase analysis, the resulting sample comprised $CuEu_2O_4$, Eu_2O_3, CeO_2 and CuO. Finally, the latter sample was subjected to reductive selenidation in a flow of H_2 and H_2Se, yielding the title quaternary selenide.

3.2. Crystal structure

The crystal structure of $EuCeCuSe_3$ was solved in orthorhombic space group *Pnma* with the cell parameters a = 1.15873(3) nm, b = 0.42274(1) nm, c = 1.19386(3) nm and V = 0.58481(2) nm^3, comprising one Eu^{2+}, one Ce^{3+}, one Cu^+ and three Se^{2-} ions in the asymmetric unit (Table 2). The DFT/PBE0-calculated cell parameters (a = 1.16213 nm, b = 0.42578 nm, c = 1.19069 nm, V = 0.58917 nm^3) are in good agreement with the experimental ones.

Table 2. Fractional atomic coordinates and isotropic displacement parameters (10^{-2} nm^2) of $EuCeCuSe_3$.

Atom	*x*	*y*	*z*	B_{iso}
Eu	0.81367(15)	0.25	0.50213(18)	0.64(10)
Ce	0.48736(14)	0.25	0.31473(16)	0.77(10)
Cu	0.2581(4)	0.75	0.2109(4)	1.45(16)
Se1	0.2216(2)	0.25	0.3077(3)	0.46(12)
Se2	0.3864(3)	0.25	0.5590(3)	0.35(12)
Se3	0.4519(3)	0.75	0.1349(3)	0.31(11)

Recently, three structural types were revealed for $EuRECuSe_3$, namely Ba_2MnS_3 for RE = La[31], Eu_2CuS_3 for RE = Sm–Y[31,43] and $KZrCuS_3$ for RE = Er–Lu[31]. In the present work, for the reported selenide $EuCeCuSe_3$ we have revealed a fourth structural type, namely $BaLaCuS_3$. Thus, the obtained crystallographic data for $EuCeCuSe_3$ allowed to supplement the previously reported results on the unit cell parameters from $r(RE^{3+})$ (Fig. 2)[32]. Notably, the same four structural types were also established for the isostructural sulfides $ARECuS_3$ (A = Sr[21], Eu[22]).

Fig. 2. Calculated (open circles) and experimental (filled circles) unit cell parameters in the crystal structures of $EuRECuSe_3$ (RE = La[31], Ce (this work), Pr[43], Nd[43], Sm[31], Eu[44], Gd–Lu[31]). Black = *a* and *b* axes for space groups *Cmcm* and *Pnma*, respectively; red = *c* and *a* axes for space groups *Cmcm* and *Pnma*, respectively; blue = *b* and *c* axes for space groups *Cmcm* and *Pnma*, respectively.

The 3D crystal structure of $EuCeCuSe_3$ is constructed from capped trigonal prisms $EuSe_7$ and $CeSe_7$ as well as $CuSe_4$ tetrahedra (Fig. 3, Table S1). The main backbone of the structure is a polymeric 3D framework $(CeSe_7)_n$, further strengthened by 1D polymeric chains $(CuSe_4)_n$, with 1D channels along the *b* axis, filled with Eu^{3+} cations (Fig. 3). Thus, for $EuRECuSe_3$ the Eu^{3+} cations are either located in the channels of the 3D frameworks (RE = La[31], Ce (this work)) or between the 2D layers (RE = Pr–Lu[31,43,44]) formed by the lanthanide- and copper-centered polyhedra.

Fig. 3. (Top) View at the crystal structure of $EuCeCuSe_3$ along the *b* axis. Color code: green polyhedral = $EuSe_7$, blue polyhedral = $CeSe_7$ and burnt orange polyhedral = $CuSe_4$. (Bottom) Coordination polyhedra formed by selenium around the metal ions in the structure of $EuCeCuSe_3$. Symmetry codes: i) x, $-1 + y$, z; ii) $1/2 - x$, $1 - y$, $1/2 + z$; iii) $1/2 - x$, $-y$, $1/2 + z$; iv) $-1/2 + x$, $1/2 - y$, $1/2 - z$; v) $1/2 - x$, $1/2 - y$, $1/2 - z$; vi) $1 - x$, $1/2 + y$, $1 - z$; vii) $1 - x$, $-1/2 + y$, $1 - z$; viii) $1/2 - x$, $1 - y$, $-1/2 + z$; ix) x, $1 + y$, z.

In the structure of $EuCeCuSe_3$, the Eu–Se bond lengths are 0.3116(3)–0.3221(3) nm, while the Ce–Se bonds are slightly shorter with 0.2980(3)–0.3142(4) nm (Table S1). The Cu–Se distances within the coordination tetrahedron vary from 0.2422(6) to 0.2468(6) nm (Table S1).

We have also compared the degree of distortion of the $CuSe_4$ coordination polyhedron in the crystal structures of the $EuRECuSe_3$ series. A tetracoordinated environment can be characterized using the so-called τ_4-descriptor[45]. The τ_4 values for perfect tetrahedral, trigonal pyramidal, seesaw and perfect square planar structures are 1.00, 0.85, 0.64–0.07 and 0.00, respectively. The τ_4 values for $EuCeCuSe_3$ and $EuLaCuSe_3$ show the lowest numbers among all the compared quaternary selenides $EuRECuSe_3$ with 0.9199 and 0.9394, respectively (Fig. 4), indicating that the coordination geometry around Cu^+ is the best described as being about 53% and 40%, respectively, along the pathway of distortion from the ideal tetrahedral toward a trigonal pyramidal structure. The τ_4 values for all selenides with the Eu_2CuS_3 structural type as well as for the erbium-based selenide, exhibing a $KZrCuS_3$ structural type, vary from 0.9702 to 0.9843 (Fig. 4), indicating only about 10%–20% distortion from the ideal tetrahedral toward a trigonal pyramidal structure. Finally, the τ_4 alues for the remaining selenides with the $KZrCuS_3$ structural type are almost 1.00 (Fig. 4), indicating an almost ideal tetrahedral coordination environment.

Fig. 4. Calculated τ_4-descriptor values for the $CuSe_4$ polyhedra in the crystal structures of the $EuRECuSe_3$ series.

Furthermore, comparison of the τ_4 value for the title selenide with those for the sulfide analogues $SrCeCuS_3$ (0.9100 and 0.9423 for two polymorphs)[19] and $EuCeCuS_3$ (0.9284 and 0.9401 for two polymorphs)[20,22,24] revealed a similar degree of distortion from the ideal tetrahedral toward a trigonal pyramidal structure.

3.3. Raman, IR and phonon spectra

As mentioned above, the crystal structure of $EuCeCuSe_3$ belongs to orthorhombic space group *Pnma* (no. 62), and its point group is D_{2h} (*mmm*). The mechanical representation consists of 72 modes, of which 3 are acoustical ones with B_{1u}, B_{2u} and B_{3u} symmetry (Table S2). The 36 Raman-active modes include 12 modes of A_g symmetry, 6 modes of B_{1g} symmetry, 12 modes of B_{2g} symmetry and 6 modes of B_{3g} symmetry, while infrared active modes include 11 modes of B_{1u} symmetry, 5 modes of B_{2u} symmetry and 11 modes of B_{3u} symmetry (acoustic modes not included) (Table S2).

A comparison of the experimental and calculated IR spectra of $EuCeCuSe_3$ as well as with the calculated IR spectrum of $CeSe_2$ has allowed to reveal characteristic modes (Fig. 5). Particularly, the most intense mode at 150 cm^{-1} corresponds to vibrations of Ce^{3+} and Se^{2-}. In general, modes at wavenumbers >200 cm^{-1} correspond to vibrations of Cu^+ and Se^{2-}, while modes at lower wavenumbers include vibrations of all the ions (Fig. 5). Participation of the atoms of $EuCeCuSe_3$ and $CeSe_2$ in the corresponding vibrations are collected in Tables S3 and S4, respectively.

Fig. 5. Experimental (black) and calculated (red) IR spectra of $EuCeCuSe_3$, and a calculated (blue) IR spectrum of $CeSe_2$.

Participation of each ion in a particular mode was estimated from the analysis of displacement vectors obtained from *ab initio* calculations with the PBE0 functional. According to the obtained results, the phonon wavenumbers at the Γ-point do not exceed 215 cm^{-1} (Fig. 6). In this range, not only the light Cu^+ and Se^{2-} ions, but also the heavy Eu^{2+} and Ce^{3+} ions are actively involved. In the crystal of $EuCeCuSe_3$, the Eu^{2+} cations actively participate in modes with wavenumbers up to about 140 cm^{-1} (Fig. 6). In general, the heavier

Eu^{2+} and Ce^{3+} cations as well as the $Se1^{2-}$ anions are more actively included in the low-wavenumber vibrations, while the Cu^{+} and $Se3^{2-}$ ions are involved in almost all modes (Fig. 6). For $Se2^{2-}$, vibration activity gradually decreases up to about 120 cm^{-1}, but it is also active at about 130–210 cm^{-1} (Fig. 6).

Fig. 6. The displacement of ions at phonon modes in $EuCeCuSe_3$.

3.4. Elastic Properties

Elastic constants of the crystal of $EuCeCuSe_3$ were calculated using the DFT/PBE0 functional, while the bulk, Young's and shear modulus were calculated in Voigt, Reuss and Hill approximations (Table 3). The dependence of the Young's modulus on the direction demonstrates the anisotropy of the elastic properties (Fig. 7). The Vickers hardness (HV) for $EuCeCuSe_3$ was calculated from the values of the shear and bulk modulus according to empirical formula $HV = 0.92(G/B)^{1.137} \times G^{0.708}$, where G is the shear modulus and B is the bulk modulus, obtained from the Hill approximation[46], yielding a value of 5.2 GPa. It was recently shown that the formula for HV is in good agreement, when hardness exceeds 5 GPa but yields overestimated values at lower hardness[46].

Table 3. Elastic constants, bulk (B), shear (G) and Young's modulus, and Vickers hardness (HV) (GPa) of $EuCeCuSe_3$.

C_{11}	C_{12}	C_{13}	C_{22}	C_{23}	C_{33}	C_{44}	C_{55}	C_{66}	HV	Averaging scheme	B	G	Young's modulus	Poisson ratio
										Voigt	77	38	98	0.289
129	43	62	138	55	110	41	45	32	5.2	Reuss	77	36	95	0.296
										Hill	77	37	96	0.293

Fig. 7. Dependence of the Young's modulus (GPa) on the direction in the crystals of $EuCeCuSe_3$.

3.5. Band structure and optical properites

We have also shed light on the band structure and density of states using the DFT calculations with hybrid PBE0 (25% HF exchange) and B3LYP (20% HF exchange) functionals as well as non-hybrid PBE functional. The corresponding calculated results of the direct band gaps for the applied functionals are similar to those and the path in the Brillouin zone is the same to that obtained recently for other quaternary selenides $EuRECuSe_3$ with space group *Pnma*[31]. Furthermore, as it was recently established for the $EuRECuSe_3$ series, the hybrid functionals overestimate the band gap, while the non-hybrid functional underestimates in comparison to the experimental value[31]. For $EuCeCuSe_3$, the experimental band gap was obtained from the Kubelka-Munk function (Fig. 8), modified for the extraction of the direct band gap as reported elsewhere[47], and amounts to 1.36 eV, which is in the range between the calculated values for different functionals (Table 4), thus also corresponding to the direct band gap.

Fig. 8. Normalized spectra of (Kubelka-Munk × Energy)^2 values plotted as a function of the incident photon energy for $EuCeCuSe_3$ (black), $EuCeCuS_3$ (red) and $EuLaCuSe_3$ (blue).

Table 4. Values of the direct band gap (eV) for $EuCeCuSe_3$, $EuCeCuS_3$ and $EuLaCuSe_3$.

Calculated for $EuCeCuSe_3$			Experimental		
$BaLaCuS_3$ structural type				Ba_2MnS_3 structural type	
PBE0 (25% HF exchange) (this work)	B3LYP (20% HF exchange) (this work)	PBE (this work)	$EuCeCuSe_3$ (this work)	$EuCeCuS_3$ (this work)	$EuLaCuSe_3$ [31]

2.34	2.21	0.90	1.36	1.46	1.54

Interestingly, comparison of the direct band gaps for the title selenide and its close analogues, namely $EuCeCuS_3$ and $EuLaCuSe_3$, allowed to reveal closely comparable values (Table 4) with the isomorphic modified Kubelka-Munk spectra (Fig. 8). Notably, replacement of Ce^{3+} with La^{3+} leads to a slightly higher increase of the direct band gap value in comparison to replacement of Se^{2-} with S^{2-} (Table 4). This can obviously be explained by isoelectronic structures of the applied chalcogenide anions, while the Ce^{3+} and La^{3+} cations have different electronic structures.

3.6. Magnetic properties

The field-dependent magnetic moment of $EuCeCuSe_3$ at 299 K is linear, which is characteristic for a paramagnet (Fig. 9). From this dependence, the effective magnetic moment and the corresponding Curie constant were calculated as 7.98 μ_B and 0.1001 $K \cdot m^3/kmol$, respectively (Table 5). The reciprocal magnetic susceptibility is well described by the Curie-Weiss law and appears to be the same in both the zero-field cooled (ZFC) and nonzero-field cooled (FC) modes (Fig. 9). As such, the C, μ and θ_p values were calculated as 0.0860 $K \cdot m^3/kmol$, 7.40 μ_B and 1.7 K, respectively, at 18–65 K (Table 5).

Fig. 9. Field-dependent magnetic moments at 299 K (a), and temperature-dependent specific magnetization and reciprocal magnetic susceptibility (b) of $EuCeCuSe_3$ at 796 A/m. The temperature-dependent measurements were performed in the zero-field cooled (ZFC) and nonzero-field cooled (FC) modes.

Experimental magnetic characteristics for $EuCeCuSe_3$, especially those obtained at low temperatures, differ significantly from the corresponding calculated parameters, obtained in the model of the free cations Eu^{2+} and Ce^{3+} (Table 5). In contrast, the experimental magnetic characteristics for the sulfide derivative $EuCeCuS_3$ at low temperatures are closely comparable with the calculated ones[24] (Table 5). This might tentatively be explained by more pronounced interactions of the magnetic active cations Eu^{2+} and Ce^{3+} through the Se^{2-} anions in the structure of $EuCeCuSe_3$ in comparison to the same interactions via the S^{2-} anions in the structure of $EuCeCuS_3$.

Table 5. Magnetic characteristics for $EuCeCuSe_3$ and $EuCeCuS_3$.

	Calculated	$EuCeCuSe_3$		$EuCeCuS_3$[24]
		Experimental at 299 K	Experimental at 18–65 K	Experimental at 20–50 K
C ($K \cdot m^3/kmol$)	0.1091	0.1001	0.0860	0.104
μ (μ_B)	8.33	7.98	7.40	–
θ_p (K)	–	–	1.7	4.8

Finally, for $EuCeCuSe_3$ the obtained θ_p value of 1.7 K is close to that of $EuCeCuS_3$ (4.8 K), for which a ferromagnetic transition was observed at 2.7 K[24]. Thus, we can tentatively suggest a similar transition for $EuCeCuSe_3$ at temperatures below 1.7 K.

4. Conclusions

In summary, we report on the novel quaternary selenide $EuCeCuSe_3$, which was synthesized from a mixture of the oxides $CuEu_2O_4$, Eu_2O_3, CeO_2 and CuO under reductive selenidation in a gas flow of H_2 and H_2Se. The applied mixture of metal oxides was before produced by thermolysis of the co-crystallized metal

nitrates, which, in turn, were obtained from a one pot reaction of Eu_2O_3, CeO_2 and Cu with concentrated nitric acid in the presence of H_2O_2. Using of the latter reagent is crucial to dissolve the poorly soluble CeO_2.

The crystal structure of the title compound, refined from the X-ray powder diffraction data, revealed that it belongs to orthorhombic space group *Pnma* with one Eu^{2+}, one Ce^{3+} and one Cu^{+} cation each as well as three Se^{2-} anions in the asymmetric unit adopting the $BaLaCuS_3$ structura type. Furthermore, the refinement of the powder pattern allows to reveal the second minor phase of $CeSe_2$ (3.3%). Thus, by the present contribution we reveal the fourth structural type within the heterometallic quartenary selenides $EuRECuSe_3$ (RE = La, Pr, Nd, Sm, Eu, Gd, Tb, Dy, Ho, Er, Tm, Yb, Lu, Y). The three-dimensional crystal structure of $EuCeCuSe_3$ is constructed from $EuSe_7$ and $CeSe_7$ capped trigonal prisms as well as $CuSe_4$ tetrahedra. Distortion of the $CuSe_4$ polyhedra was compared for a whole $EuRECuSe_3$ series using the τ_4-descriptor for four coordinated ions, which reveals the highest degree of distortion for the cerium-containing selenide, followed by the lanthanum-based derivative.

The experimental IR spectrum of the synthesized sample was interpreted using the calculated IR spectra of $EuCeCuSe_3$ and $CeSe_2$. The theoretical calculations also allow to assign vibrational modes as well as to reveal involved ions responsible for the corresponding modes.

Optical properties of $EuCeCuSe_3$ were revealed by diffuse reflectance spectroscopy further verified by DFT calculations using both the hybrid PBE0 (25% HF exchange) and B3LYP (20% HF exchange) as well as non-hybrid PBE functionals. The experimental direct band gap of the reported quaternary selenide was found to be 1.36 eV, which is slightly lower in comparison to those of close analogues, such as $EuCeCuS_3$ (1.46 eV) and $EuLaCuS_3$ (1.54 eV).

Finally, the title compound is paramagnetic above 4 K, with the possible ferromagnetic transformation at lower temperatures, and its magnetic properies are similar to those of the sulfide analogue $EuCeCuS_3$.

References

[1] Kamarzin AA, Mironov KE, Sokolov VV, Malovitsky YN, Vasil'yeva IG. Growth and properties of lanthanum and rare-earth metal sesquisulfide crystals. J Cryst Growth. 1981;52:619.

[2] Zhuze VP, Shelykh AI. Optical properties and electronic structure of sesquisulfides and oxides of rare earth metals. Fiz Tekh Poluprovodn. 1989;23:393. (in Russ.)

[3] Prokofiev AV, Shelykh AI, Golubkov AV, Smirnov IA. Crystal growth and optical properties of rare earth sesquiselenides and sesquisulphides – new magneto-optic materials. J Alloys Compd. 1995;219:172.

[4] Li L, Wang H, Zou L, Wang X. Controllable synthesis, photocatalytic and electrocatalytic properties of CeO_2 nanocrystals, RSC Adv. 2015;5(52):41506.

[5] Ma R, Jahurul Islam M, Amaranatha Reddy D, Kim TK. Transformation of CeO_2 into a mixed phase CeO_2/Ce_2O_3 nanohybrid by liquid phase pulsed laser ablation for enhanced photocatalytic activity through Z-scheme pattern. Ceram Int. 2016;42(16):18495.

[6] Ivanova AS. Physicochemical and catalytic properties of systems based on CeO_2. Kinet Catal. 2009;50: 797.

[7] Wan J, Liu Y, Zhou Y, Liu H, Wu G, Kan J et al. Controllable synthesis of argentum decorated $CuO_x@CeO_2$ catalyst and its highly efficient performance for soot oxidation. J Rare Earths 2022;40(10):1546.

[8] Chang Sh, Jia Y, Zeng Y, Qian F, Guo L, Wu Sh, Lu J. Effect of interaction between different CeO_2 plane and platinum nanoparticles on catalytic activity of Pt/CeO_2 in toluene oxidation. J Rare Earths 2022;40(11):1743.

[9] Westrum EF, Burriel R, Gruber JB, Palmer PE, Beaudry BJ, Plautz WA. Thermophysical properties of the lanthanide sesquisulfides. I. Schottky functions and magnetic and electronic properties of γ-La_2S_3, γ-Ce_2S_3, γ-Nd_2S_3, and γ-Gd_2S_3. J Chem Phys. 1989;91(8):4838.

[10] Shelykh AI, Prokof'ev AV, Melekh BT. Band gap variation in Ln_2X_3 compounds (Ln = Rare earth element, X = O, S, Se). Phys Solid State 1996;38:427.

[11] Patschke R, Heising J, Kanatzidis M, Brazis P, Kannewurf CR. $KCuCeTe_4$: A New Intergrowth Rare Earth Telluride with an Incommensurate Superstructure Associated with a Distorted Square Net of Tellurium. Chem Mater. 1998;10(3):695.

[12] Sutorik AC, Albritton-Thomas J, Kannewurf CR, Kanatzidis MG. The First Examples of Alkali Metal/Cu/Ce/Chalcogenides: On the Layered Heterometallic Compounds $KCuCe_2S_6$ and $K_2Cu_2CeS_4$. J Am Chem Soc. 1994;116(17):7706.

[13] Wu P, Christuk AE, Ibers JA. New Quaternary Chalcogenides $BaLnMQ_3$ (Ln = Rare Earth or Sc; M = Cu, Ag; Q = S, Se). Structure and Property Variation vs Rare-Earth Element. J Solid State Chem. 1994;110:337.

[14] Sutorik AC, Albritton-Thomas J, Hogan T, Kannewurf CR, Kanatzidis M.G. New Quaternary Compounds Resulting from the Reaction of Copper and *f*-Block Metals in Molten Polychalcogenide Salts at Intermediate Temperatures. Valence Fluctuations in the Layered $CsCuCeS_3$. Chem Mater. 1996;8:751.

[15] Klawitter Y, Nather C, Jeb I, Bensch W, Kanatzidis MG. The superstructure of $KCuCe_2Se_6$ due to ordering of copper cations. Solid State Sci. 1999;1:421.

[16] Strobel S, Schleid Th. Quaternary strontium copper(I) lanthanoid(III) selenides with cerium and praseodymium: $SrCuCeSe_3$ and $SrCuPrSe_3$, unequal brother and sister. Z Naturforsch. 2004;59b:985.

[17] Strobel S. Darstellungsmethoden und Kristallstrukturen ternärer Münzmetall-Lanthanid-Chalkogenide und quaternärer Kupfer-Lanthanid-Selenide mit Alkali- und Erdalkalimetallen. Stuttgart University, Stuttgart, Germany, 2005.

[18] Babo J-M, Albrecht-Schmitt TE. $Ce_2AgYb_{5/3}Se_6$, $La_2CuErTe_5$, and $Ce_2CuTmTe_5$: Three new quaternary interlanthanide chalcogenides. J Solid State Chem. 2013;197:414.

[19] Ruseikina AV, Solov'ev LA. Crystal Structures of *α*- and *β*-$SrCeCuS_3$. Russ J Inorg Chem. 2016;61(4): 482.

[20] Ruseikina AV. Crystal structure of $EuCeCuS_3$. Russ J Inorg Chem. 2016;61(11):1403. [21] Ruseikina AV, Andreev OV, Galenko EO, Koltsov SI. Trends in thermodynamic parameters of phase transitions of lanthanide sulfides $SrLnCuS_3$ (Ln = La–Lu). J Therm Anal Calorim. 2017;128(2):993.

[22] Ruseikina AV, Andreev OV. Regularities of change in the structural parameters of $EuLnCuS_3$ (Ln = La–Nd, Sm, Gd, Ho). Russ J Inorg Chem. 2017;62(2):160.
[23] Pomelova TA, Podlipskaya TYu, Kuratieva NV, Cherkov AG, Nebogatikova NA, Ryzhikov MR et al. Synthesis, Crystal Structure, and Liquid Exfoliation of Layered Lanthanide Sulfides KLn_2CuS_6 (Ln = La, Ce, Pr, Nd, Sm). Inorg Chem. 2018;57:13594.
[24] Ruseikina AV, Chernyshev VA, Velikanov DA, Aleksandrovsky AS, Shestakov NP, Molokeev MS et al. Regularities of the property changes in the compounds $EuLnCuS_3$ (Ln = La–Lu). J Alloys Compd. 2021;874:159968.
[25] Iyer AK, Rudyk BW, Lin X, Singh H, Sharma AZ, Wiebe ChR et al. Noncentrosymmetric rare-earth copper gallium chalcogenides $RE_3CuGaCh_7$ (RE = La–Nd; Ch = S, Se): An unexpected combination. J Solid State Chem. 2015;229:150.
[26] Koscielski LA, Ibers JA. The structural chemistry of quaternary chalcogenides of the type AMM'Q_3. Z Anorg Allg Chem. 2012;638:2585.
[27] Patschke R, Brazis P, Kannewurf CR, Kanatzidis M. $Rb_2Cu_3CeTe_5$: a quaternary semiconducting compound with a two-dimensional polytelluride framework. J Mater Chem. 1998;8:2587.
[28] Jin GB, Choi ES, Guertin RP, Booth CH, Albrecht-Schmitt ThE. Syntheses, Structure, Magnetism, and Optical Properties of the Ordered Interlanthanide Copper Chalcogenides Ln_2YbCuQ_5 (Ln = La, Ce, Pr, Nd, Sm; Q = S, Se): Evidence for Unusual Magnetic Ordering in Sm_2YbCuS_5. Chem Mater. 2011;23: 1306.
[29] Pal K, Xia Yi, Shen J, He J, Luo Yu, Kanatzidis MG, Wolverton Ch. Accelerated discovery of a large family of quaternary chalcogenides with very low lattice thermal conductivity. Comput Mater. 2021;7:82.
[30] Ruseikina AV, Molokeev MS, Chernyshev VA, Aleksandrovsky AS, Krylov AS, Krylova SN et al. Synthesis, structure, and properties of $EuScCuS_3$ and $SrScCuS_3$. J Solid State Chem. 2021;296:121926.
[31] Grigoriev MV, Solovyov LA, Ruseikina AV, Aleksandrovsky AS, Chernyshev VA, Velikanov DA et al. Quaternary Selenides $EuLnCuSe_3$: Synthesis, Structures, Properties and In Silico Studies. Int J Mol Sci. 2022;23(3):1503.
[32] Serebrennikov VV. The Chemistry of the Rare-earth Elements (Scandium, yttrium, lanthanides). Tomsk: Tomsk University Press, 1961.
[33] Christuk AE, Wu P, Ibers JA, New Quaternary Chalcogenides $BaLnMQ_3$ (Ln - Rare Earth; M = Cu, Ag; Q = S, Se): I. Structures and Grinding-Induced Phase Transition in $BaLaCuQ_3$. J Solid State Chem. 1994;110:330.
[34] Bruker AXS TOPAS V4: General profile and structure analysis software for powder diffraction data. – User's Manual. Bruker AXS, Karlsruhe, Germany. 2008.
[35] Pennington WT. DIAMOND – Visual Crystal Structure Information System. J Appl Crystallogr. 1999;32:1028.
[36] Velikanov DA. High-Sensitivity measurements of the magnetic properties of materials at cryogenic temperatures. Inorg Mater Appl Res. 2020;11:801.
[37] Velikanov DA. Magnetometer with a Superconducting Quantum Interferometric Sensor. RF Pat. 2481591. 2013. http://www.freepatent.ru/patents/2481591 (accessed 19 June 2022).
[38] Velikanov DA. Vibration Magnetometer. RF Pat. 2341810. 2008. http://www.freepatent.ru/patents/2341810 (accessed 19 June 2022).
[39] Crystal. http://www.crystal.unito.it/index.php (accessed 19 June 2022).
[40] Energy-consistent Pseudopotentials of the Stuttgart/Cologne Group. http://www.tc.uni-koeln.de/PP/clickpse.en.html (accessed 19 June 2022).
[41] Kochedigov VA, Zakiryanova ID, Korzun IV. Research of thermal dissociation of interaction products of rare-earth element oxides with the components of atmospheric air. Anal Control. 2005;9:58.
[42] Komissarova LN, Shatskii VM, Pushkina GYa, Shcherbakova LG, Mamsurova LG, Sukhanova GE. Compounds of Rare-Earth Elements: Carbonates, Oxalates, Nitrates, and Titanates. Edited by Tananaev IV, Buslaev YuA. Moscow: Nauka, 1984.
[43] Grigoriev MV, Locke R, Ruseikina AV, Schleid TH. Crystal structure of compounds $EuPrCuSe_3$ and $EuNdCuSe_3$. XXXII Russian Youth Scientific Conference Problems of Theoretical and Experimental Chemistry. Yekaterinburg, Russia, 2022.
[44] Gladisch FC, Maier S, Steinberg S. Eu_2CuSe_3 revisited by means of experimental and quantum-chemical techniques. Eur J Inorg Chem. 2021;15:1510.

[45] Yang L, Powell DR, Houser RP. Structural variation in copper(I) complexes with pyridylmethylamide ligands: structural analysis with a new four-coordinate geometry index, τ_4. Dalton Trans. 2007;9:955.

[46] Tian Y, Xu B, Zhao Zh. Microscopic theory of hardness and design of novel superhard crystals. Int J Refract Met Hard Mater. 2012;33:93.

[47] Landi S, Segundo IR, Freitas E, Vasilevskiy M, Carneiro J, Tavares CJ. Use and misuse of the Kubelka-Munk function to obtain the band gap energy from diffuse reflectance measurements. Solid State Commun. 2022;341:114573.

Graphical abstract: We report in-depth structural, optical, magnetic and computational studies of the novel quaternary selenide $EuCeCuSe_3$.

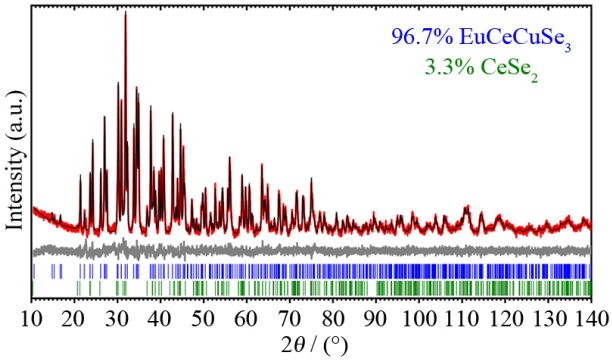

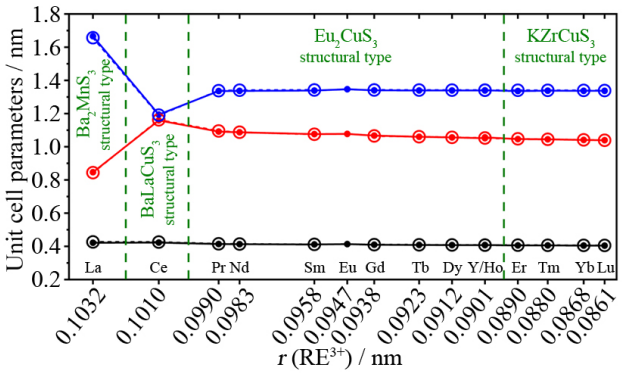

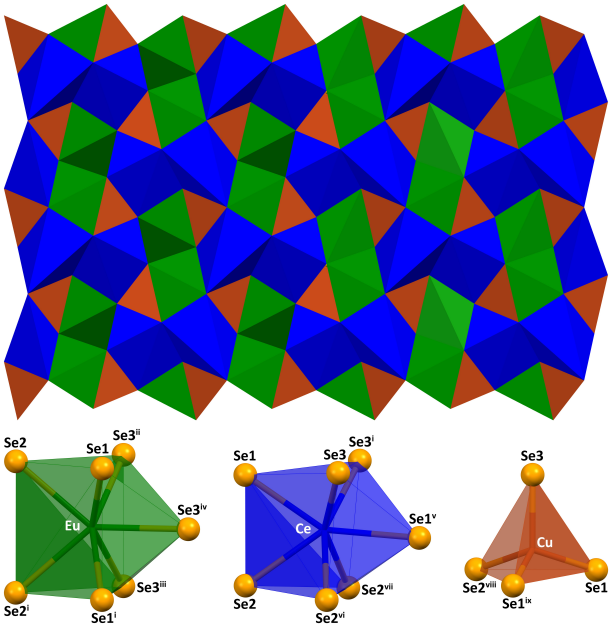

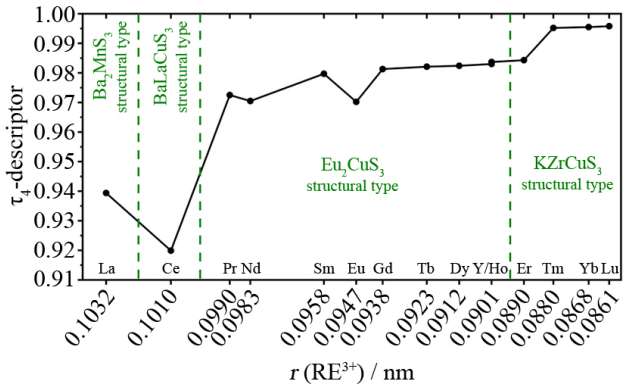

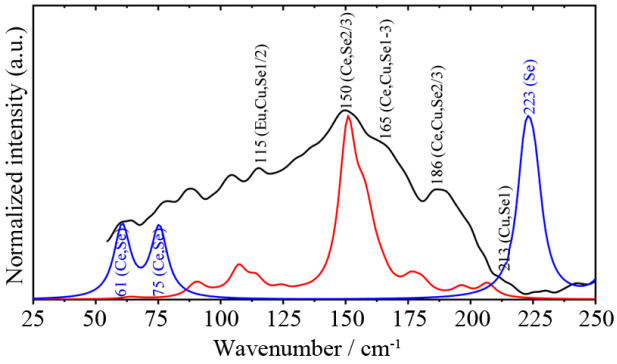

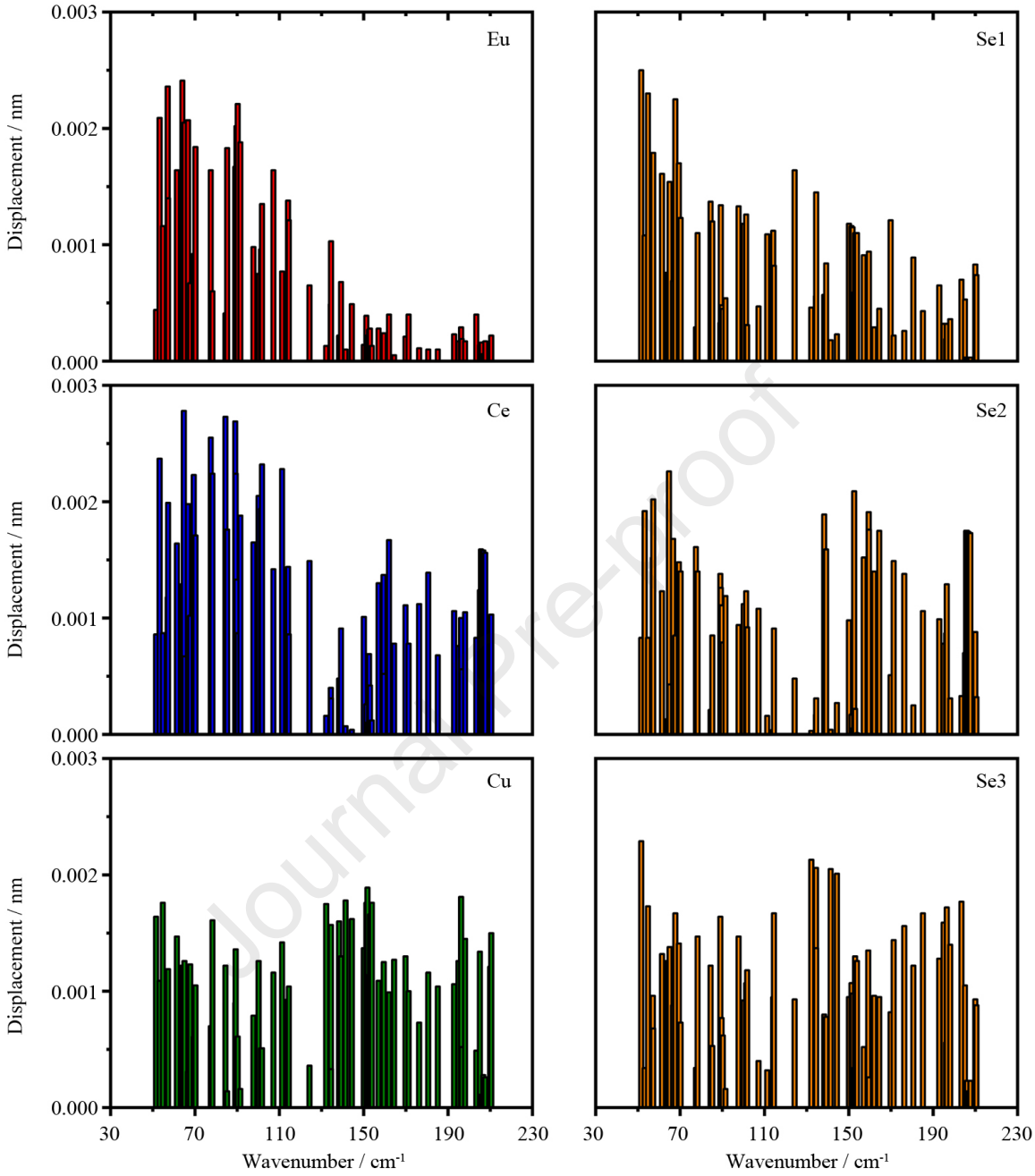

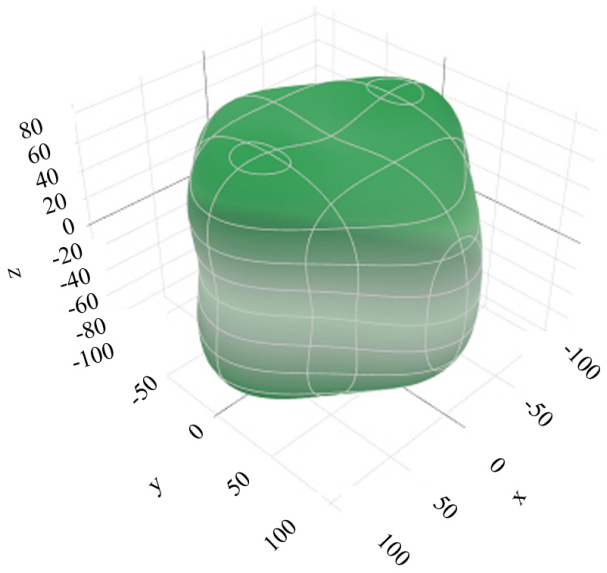

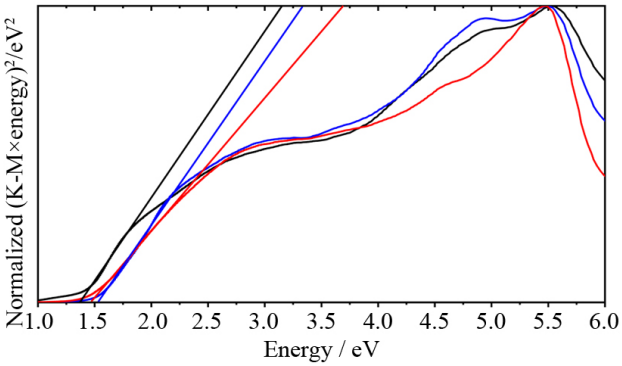

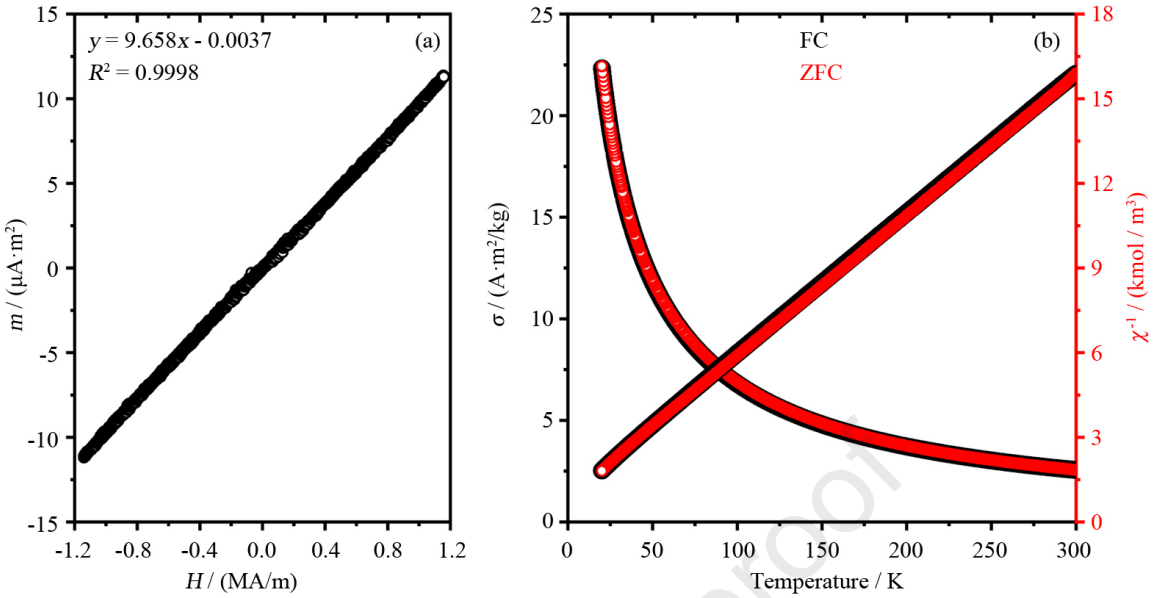

We report on the novel quaternary selenide $EuCeCuSe_3$

The crystal structure of $EuCeCuSe_3$ was elucidated from X-ray powder diffraction

Magnetic and optical properties of $EuCeCuSe_3$ were revealed

Theoretical calculations were performed to verify the structure and properties of $EuCeCuSe_3$

There are no conflicts to declare.